

angles for the scattered beam. In other words, this theory predicts that the scattered beam has a maximum of intensity at right angles to the incident beam. As an aid to the interpretation of this result, one can strongly contend that the incident electron must be captured into the p orbital Ψ_{210} which is oriented parallel to the initial direction of approach \vec{k}_0 . In the final $(2p)^2\ ^3P_g$ state, the other bound electron must therefore lie in one of the p orbitals Ψ_{21-1} or Ψ_{211} oriented perpendicular to \vec{k}_0 . Consequently, due to the preferential ejection of the third electron (induced by the perturbation $1/r_{23}$), it can be argued that the intermediate complex, a helium negative ion, is composed of a doubly occupied Ψ_{211} or Ψ_{21-1} orbital and a singly occupied Ψ_{210} orbital.

The total cross section $\sigma = 2\iint I(\theta, \phi) d\phi d\theta \sin\theta$ shows the fairly sharp peak and rapid decay with increased incident electron energy characteristic of exchange reactions. In Fig. 1 the cross section for the transition is compared with other processes.

Even though the Born-Oppenheimer approximation is not very accurate, and the helium wave functions are not very good, the results suggest that the experiments be run, perhaps after the manner of Swift and Whiddington,⁷ looking for a transition with the properties described. In order

that a better prediction may be made, further calculations are in progress using better atomic wave functions and the more accurate distorted-wave and strong-coupling scattering theories.

The authors wish to thank the Numerical Analysis Center of the University of Minnesota for the use of the Control Data 1604 computer, and the National Science Foundation for partial support of this research.

¹B. H. Bransden and A. Dalgarno, Proc. Phys. Soc. (London) **66**, 904, 911 (1953). These authors also summarize the literature on doubly excited states.

²E. Holøien, J. Chem. Phys. **33**, 301 (1960); G. Herzberg, *Atomic Spectra and Atomic Structure* (Dover Publications, New York, 1944), pp. 167, 171.

³E. Holøien, J. Chem. Phys. **29**, 676 (1958).

⁴C. E. Moore, *Atomic Energy Levels*, National Bureau of Standards Circular No. 467 (U. S. Government Printing Office, Washington, D. C., 1949), Vol. 1, p. 4.

⁵H. Massey and B. L. Moiseiwitsch, Proc. Roy. Soc. (London) **A258**, 147 (1960).

⁶C. Eckart, Phys. Rev. **36**, 878 (1930). Both the authors and B. L. Moiseiwitsch [*Quantum Theory*, edited by D. R. Bates (Academic Press, Inc., New York, 1961), Vol. 1, p. 223] have corrected a slight error in Eckart's values.

⁷W. Swift and R. Whiddington, Proc. Leeds Phil. Lit. Soc., Sci. Sect. **3**, 262 (1937).

ELECTROMAGNETIC STRUCTURE OF THE GIANT DIPOLE RESONANCE*

F. H. Lewis, Jr., and J. D. Walecka[†]

Institute of Theoretical Physics, Department of Physics, Stanford University, Stanford, California

and

J. Goldemberg and W. C. Barber

High-Energy Physics Laboratory, Stanford University, Stanford, California

(Received 24 April 1963)

Inelastic electron scattering yields valuable information about the spatial nature of the transition charge, current, and magnetization densities in nuclei. Since the electron part of the process is completely calculable, one can directly compare the experimental inelastic form factors (functions of the momentum transferred to the nucleus) with the predictions of nuclear theory. Different nuclear models can give quite different behavior for these form factors, and thus electron scattering provides a unique tool for elucidating nuclear structure. We wish to present some experimental and theoretical results on the nature of the giant

dipole resonance in C^{12} illustrating these points.

The differential cross section at 180° for electron excitation of the giant dipole resonance is given in first Born approximation ($Z/137 \ll 1$) by¹

$$\frac{d\sigma}{d\Omega} = \frac{16\pi\alpha^2 K_2^2}{\Delta^4} \left| \langle J=1^- || T_1^{\text{el}}(q) || J=0^+ \rangle \right|^2, \quad (1)$$

where K_2 is the final electron wave number, $\hbar\vec{q}$ and $\hbar\Delta$ are the three- and four-momenta transferred to the nucleus, and we have neglected the electron mass and nuclear recoil. One needs the reduced transition matrix element (the "inelastic form factor") of the transverse electric dipole

operator,^{1,2}

$$T_{1M}^{el}(q) = \frac{1}{q} \int d\vec{x} \{ \vec{j}_N(\vec{x}) \cdot [\vec{\nabla} \times j_1(qx) \vec{Y}_{111}^M(\Omega_x)] + q^2 \vec{\mu}_N(\vec{x}) \cdot [j_1(qx) \vec{Y}_{111}^M(\Omega_x)] \}, \quad (2)$$

where $e\vec{j}_N(\vec{x})$ and $e\vec{\mu}_N(\vec{x})$ are the nuclear current and magnetization density operators.

The same operator describes the emission and absorption of electric dipole γ rays by nuclei, only in that case a single fixed value of q appears, $q = q_{10} = E_{10}/\hbar c$, where E_{10} is the excitation energy. The integrated photoabsorption cross section for reactions proceeding through the giant resonance is

$$\int \sigma_{abs}(E) dE = (2\pi)^3 \alpha \frac{(\hbar c)^2}{E_{10}} \left| \langle 1^- || T_1^{el}(q_{10}) || 0^+ \rangle \right|^2. \quad (3)$$

Note that for small q_{10} one has the familiar expression

$$T_{1M}^{el}(q_{10}) \rightarrow -\frac{\sqrt{2}}{3} q_{10} \int d\vec{x} x \rho_N(\vec{x}) Y_{1M}(\Omega_x),$$

where $e\rho_N(\vec{x})$ is the nuclear charge density operator. For larger values of \vec{q} , the operator is sensitive to details of the current and magnetization [Eq. (2)].

We have calculated the inelastic form factors for several models of the giant resonance. The Goldhaber-Teller model³ calculation is described in reference 1. The hydrodynamical model⁴ has been studied and yields a matrix element proportional to $j_1(qR)/qR$, where R is the nuclear radius. Calculations similar to those of Brown et al.⁵ have also been carried out for C^{12} keeping the four lowest energy particle-hole states $(1d_{3/2})^{-1}(1p_{3/2})^{-1}$, $(1d_{5/2})^{-1}(1p_{3/2})^{-1}$, $(2s_{1/2})^{-1}(1p_{3/2})^{-1}$, and $(1p_{1/2})^{-1}(1s_{1/2})^{-1}$, all coupled to $J=1^-$, $T=1$. The residual interaction

$$V_{res} = \sum_{i < j} V(ij) - \sum_i U(|\vec{r}_i|),$$

where $U(|\vec{r}_i|)$ is the self-consistent central potential and $V(1, 2) = -v_0[(1 - \eta) + \eta \vec{\sigma}_1 \cdot \vec{\sigma}_2] \delta(\vec{r}_1 - \vec{r}_2)$, was diagonalized among these states, the configuration energies being taken from experiment as in reference 5. Harmonic oscillator wave functions were used to compute radial matrix elements. $\eta = 0.064$ was chosen to give the same singlet/triplet ratio as in the free interaction, and $v_0 = 410 \text{ MeV F}^3$ was chosen to fit the known $J=1^-$, $T=1$ states in C^{12} (it is about the same value as in reference 5). We find one state at 18.3 MeV corresponding to the

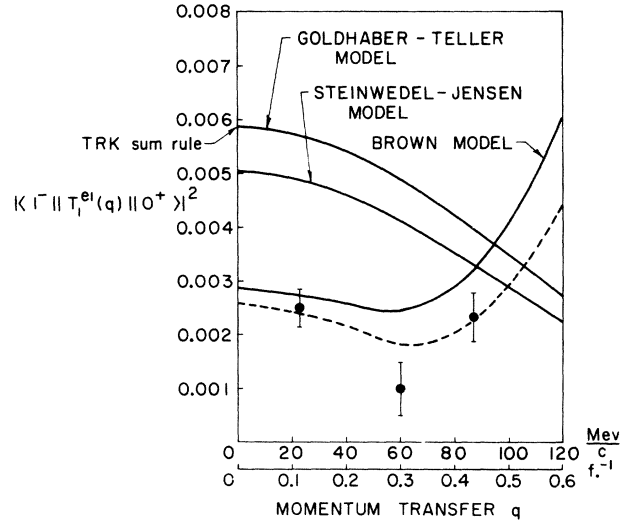


FIG. 1. Form factor vs q for the giant dipole resonance in C^{12} . The dashed curve is discussed in reference 8. We have also indicated the value corresponding to the Thomas-Reiche-Kuhn sum rule.

observed state at 17.6 MeV,⁶ two states at 21.1 MeV and 23.7 MeV, which we interpret as the giant resonance observed in electron scattering in the region 21-26 MeV (note these states have not been resolved; therefore they presumably have large overlapping widths), and a state at 33.6 MeV which has not been observed. The parameters are now fixed and the cross section we compute is the sum of the cross sections to the two levels at 21.1 and 23.7 MeV. The results for all three models are shown in Fig. 1.

The excitation of the giant resonance by inelastic electron scattering in carbon was measured at 180° using electrons from the Stanford Mark II linear accelerator. The apparatus has been described before^{7,1}; a measurement of the giant resonance cross section at an incident energy of 40 MeV was described previously.¹ For the present experiments an additional 10-foot accelerator section was installed in the Mark II accelerator to permit work at energies up to 60 MeV.

Figure 2 shows typical results obtained for carbon at 55 MeV; a graphite target 0.009 radiation length thick was used; the absolute cross sections were determined by comparison with the proton cross section as in reference 1. An elastic peak for carbon is seen because the finite aperture of the spectrometer and multiple scattering of the electrons in the target admit particles scattered near 180° ; the well-known $M1$ transition to the

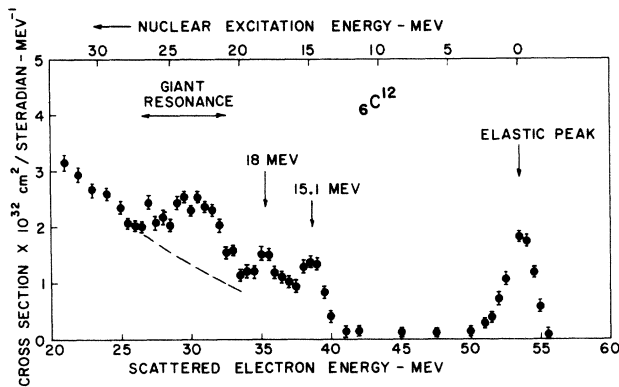


FIG. 2. Spectrum of 55-MeV electrons scattered at 180° by C^{12} ; the radiation tail was not unfolded in this curve.

15.1-MeV level in carbon is also clearly seen as expected. At ~ 18 MeV some evidence for a broad level is present, and at ~ 23 MeV a large bump is observed which is attributed to excitation of the "giant resonance." The points shown in Fig. 1 for the inelastic electron scattering reduced matrix elements were derived from the area under the "giant resonance" region. The point at $q = 60$ MeV/c was taken from reference 1, and the point $q = 87$ MeV/c was obtained from Fig. 2 of this paper after subtracting a background shown by the dashed line on Fig. 2. The subtraction was made in a similar way in reference 1, and although absolute values are somewhat uncertain, there is no doubt that the experimental value of the matrix element increases as q increases from 60 to 90 MeV/c.

The point at 23 MeV was obtained by adding averages of the various reported measurements of the integrated cross section for (γ, n) and (γ, p) reactions. The contribution of the 17.6-MeV level was calculated from $B^{11}(p, \gamma_0)C^{12}$ and detailed balance (it is $\sim 5\%$) and then subtracted.

In Fig. 1 we see that the collective models and the shell model give completely different behavior for the inelastic form factor. The shell model predicts quite an unusual behavior, as there is a pronounced dip in the form factor within a span of $\hbar c q < 100$ MeV. This results from the fact that there are two states involved and the form factor

to the first is decreasing while that to the second is increasing (note this also predicts a shift to higher energy in the position of the resonance which is observed). The experiments also quite clearly show this dip. The shape of the shell-model form factor is relatively insensitive to the values of ν_0 and η . The main role of the two-particle force is to get the levels at the right energy. There is, however, a fairly sizable contribution at large q from the unperturbed $(1p_{1/2})(1s_{1/2})^{-1}1^-; 1$ state (which has a very large unperturbed configuration energy),⁸ indicating that a quantitative fit to the form factor would be sensitive to small admixtures of states in the wave function. The conclusion is that the shell-model states and operators yield the rather remarkable form factor obtained experimentally, while the collective models are completely inadequate for describing these nuclear states in any detail.

We are indebted to W. Czyz for many stimulating discussions.

*This work was supported in part by the U. S. Office of Naval Research, the U. S. Atomic Energy Commission, and the U. S. Air Force through the Air Force Office of Scientific Research under contract AF 49(638)-388.

[†]A. P. Sloan Foundation Fellow.

¹J. Goldemberg, Y. Torizuka, W. C. Barber, and J. D. Walecka (to be published).

²The notation follows A. R. Edmonds, *Angular Momentum in Quantum Mechanics* (Princeton University Press, Princeton, New Jersey, 1960).

³M. Goldhaber and E. Teller, *Phys. Rev.* **74**, 1046 (1948).

⁴H. Steinwedel and J. H. D. Jensen, *Z. Naturforsch.* **59**, 413 (1950).

⁵G. E. Brown, L. Castillejo, and J. A. Evans, *Nucl. Phys.* **22**, 1 (1961); G. E. Brown and N. Vinh Mau, *Nucl. Phys.* **29**, 89 (1962).

⁶T. Lauritsen and F. Ajzenberg-Selove, *Nuclear Data Sheets* (National Academy of Science and National Research Council, Washington, D. C., 1962).

⁷G. A. Peterson and W. C. Barber, *Phys. Rev.* **128**, 812 (1962).

⁸In Fig. 1, we have also plotted the results one would get by leaving this high-lying unperturbed state out of the calculation completely.